MATERIALS CHEMISTRY FRONTIERS

CCS 中国化学会 CHINESE CHEMICAL SOCIETY

ICCAS

ROYAL SOCIETY OF CHEMISTRY

Triphenylene Containing Blue-Light Emitting Semi-fluorinated Aryl Ether Polymers with Excellent Thermal and Photostability

Journal:	*Materials Chemistry Frontiers*
Manuscript ID	QM-RES-02-2022-000099.R1
Article Type:	Research Article
Date Submitted by the Author:	22-Mar-2022
Complete List of Authors:	Shelar, Ketki; Mississippi State University, Chemistry Le, Nghia; Vietnam National University Ho Chi Minh City, chemistry; Mississippi State University, Mukeba, Karl; Mississippi State University, Chemistry Dey, Sriloy; Mississippi State University Farajidizaji, Behzad; Mississippi State University, Chemistry Athukorale, Sumudu; Mississippi State University, Chemistry Pittman, Jr., Charles; Mississippi State University, Chemistry; Northeast Forestry University, Biomass Material Engineering Webster, Charles Edwin; Mississippi State University, Chemistry Donnadieu, Bruno; Mississippi State University, Department of Chemistry Caldona, Eugene; Mississippi State University Smith, Dennis; Mississippi State University

Triphenylene Containing Blue-Light Emitting Semi-fluorinated Aryl Ether Polymers with Excellent Thermal and Photostability

Ketki Eknath Shelar, Nghia Le, Karl M. Mukeba, Sriloy Dey, Behzad Farajidizaji, Sumudu Athukorale, Charles U. Pittman, Jr., Charles Edwin Webster, Bruno Donnadieu, Eugene Caldona, Dennis W. Smith, Jr.*

Department of Chemistry and MSU Advanced Composites Institute, Mississippi State University, Starkville, MS 39759.

[*] To whom correspondence should be addressed:
Prof. Dennis W. Smith, Jr., Ph.D.
Department of Chemistry,
Mississippi State University, MS State, MS-39762,
Email: dsmith@chemistry.msstate.edu,
Ph: +1-662-325-7813

Abstract

Integration of polycyclic aromatic hydrocarbon (PAH) units into semi-fluorinated polymers affords high thermal stability and excellent processability for potential applications in optoelectronic, gas-separation, and advanced composites. Base-promoted step-growth polycondensation of commercial bisphenols with new triphenylene containing *bis*-trifluorovinyl ether (TFVE) monomers afford semi-fluorinated arylene vinylene ether (FAVE) polymers in good yields. The solution-processable polymers form tough transparent films and produced substitution dependent blue-light emission in solution with emission quantum yields ranging from 7.2-12% (in dichloromethane). Although predominantly amorphous with high glass transition temperatures (T_g) ranging from 176-243 °C, powder X-ray diffraction studies show typical molecular diameter and pi-stacking reflections for triphenylene polymers. The polymers exhibited excellent thermal stability, solution photostability, and remarkable thermal oxidative photostability after heating at 250 °C for 24 h in air. Further, a model post-polymerization Scholl coupling afforded a novel semi-fluorinated hexabenzocoronene polymer with new optical properties. Time-dependent density functional theory (TD-DFT) computations were also performed using SMD (dichloromethane)-ωB97XD/BS1 (BS1 = 6-31G(d') for C, H, O and F). This work demonstrated the synthesis and characterization of processable, blue-light emitting, thermally stable triphenylene enchained semi-fluorinated aryl ether polymers.

Keywords

Semi-fluorinated polymers, aromatic ether polymers, triphenylene polymers, blue light emitters, time-dependent density functional theory (TD-DFT), fluorinated arylene vinylene ethers (FAVE) polymers, thermally stable polymers.

Introduction

Fluorine imparts enhanced properties to polymeric materials targeted for high performance or extreme conditions such as those needed for protective coatings, optoelectronic thin films, biomedical devices, aerospace materials, gas-separation membranes, and fuel cell applications.[1–3] The growing organic electronics industry has long sought extremely durable, lightweight, and cheap optoelectronic devices (e.g., OLEDs, organic photovoltaics (OPVs), and organic field-effect transistors (OFETs)) with high luminance at low voltage, and high color purity.[4,5] Translating the organic light-emitting diode (OLED) performance of fragile organometallics (such as Alq3 by Kodak in 1987[6]) into robust polymers with real macromolecular properties continues to be a "holy grail" for organic electronics.[7,8] In contrast to small-molecules for optoelectronic applications, polymers possess film-forming capability, solution-processability and high thermal stability with more control in tuning desired optoelectronic properties.[9]

The pioneering research of graphene towards molecular electronics led to the study of various polyaromatic hydrocarbons (PAH). They can be used for bottom-up synthesis to solution-processable nanographenes with band gap tunability for optoelectronic applications.[10-12] Polymers containing PAHs range from completely amorphous to crystalline nature and have attracted attention for the development of supercapacitors,[13] transistors,[14] solar cells,[15] semiconductor,[10] blue-light emitting lasers,[16] photovoltaics[17] etc. Numerous reports exist on stable red and green light-emitting devices.[18–23] However, the development of reliable and efficient blue light OLEDs is still challenging.[24–26] The poly(*para*-phenylene) (PPP)[27,28] and fluorene[29] homo/copolymers are commonly used in solution-processed blue OLEDs. However, long-term stability concerns, due to the poor charge injection/transport[30] and oxidization of the bridge head positions[31] of some PPP

and fluorene-based emitters, necessitate the quest for improved oligomeric and polymeric light-emitting materials.[32–35]

In 1978, triphenylene was discovered as a member of the discotic liquid crystal core family.[36] Various triphenylenes are easy to synthesize, and have interesting charge migration,[37] electroluminescence,[38] surface self-assembly,[39] ferroelectric switching,[40] and alignment[41] properties. Triphenylenes have been polymerized in various ways, including Suzuki-Miyaura[42] and Sonogoshira[43] coupling. Triphenylene materials have applications in photoconductors, photovoltaic solar cells, gas sensors, and light-emitting diodes.

Low polarizability, induced C-C electronegativity, and the high C-F bond strengths all contribute to the exceptional properties of fluoropolymers.[33,34] Synthetic versatility allows tailoring of fluorinated polymer structures, varying their properties for desired applications. These properties include optical, excellent thermal stability, chemical resistance, low refractive index, and low surface energy.[35–37] Unlike fully fluorinated or highly fluorinated polymers, semi-fluorinated polymers generally exhibit better solubility.[49] The enchainment of polycyclic aromatic hydrocarbon (PAH) units (such as hexabenzocoronene,[50] acenaphthenequinone,[51] phenanthrenequinone,[52,53] and triphenylene[54]) afforded a new class of semi-fluorinated polymers for potential applications in optoelectronic, gas-separation, and advanced composites (Figure 1). Recently, our research group has reported triphenylene-enchained semi-fluorinated polymers as an extension to a general platform to combine property driving PAH core segments within robust and processable fluoropolymers.[54] Perfluorocyclobutyl (PFCB) aromatic ether polymers were obtained via [2+2] radical-mediated thermal cyclopolymerization of triphenylene-enchained monomers containing trifluorovinylether (TFVE) end groups (Figure 1). PFCB aryl ether polymers containing triphenylene were readily soluble in common organic solvents and had unprecedented

glass transition temperatures up to 295 °C. Furthermore, in both solid and solution states, these polymers emit blue light. Even after being heated 24 h in air to 250 °C in air, their blue light emission after cooling remained unchanged, demonstrating their exceptional thermal-oxidative stability.

This work presents the robust, transition metal-free, step-growth condensation polymerization of commercial bisphenols with *bis*-trifluorovinyl aryl ether (*bis*-TFVE) monomers, containing substituted triphenylene cores to generate fluorinated aryl vinylene ether (FAVE) polymers (Figure 1). Base-mediated nucleophilic addition/elimination polymerization produces processable FAVE polymers containing reactive fluoroalkenes in the backbone available for post-functionalization and/or cross-linking.[55]

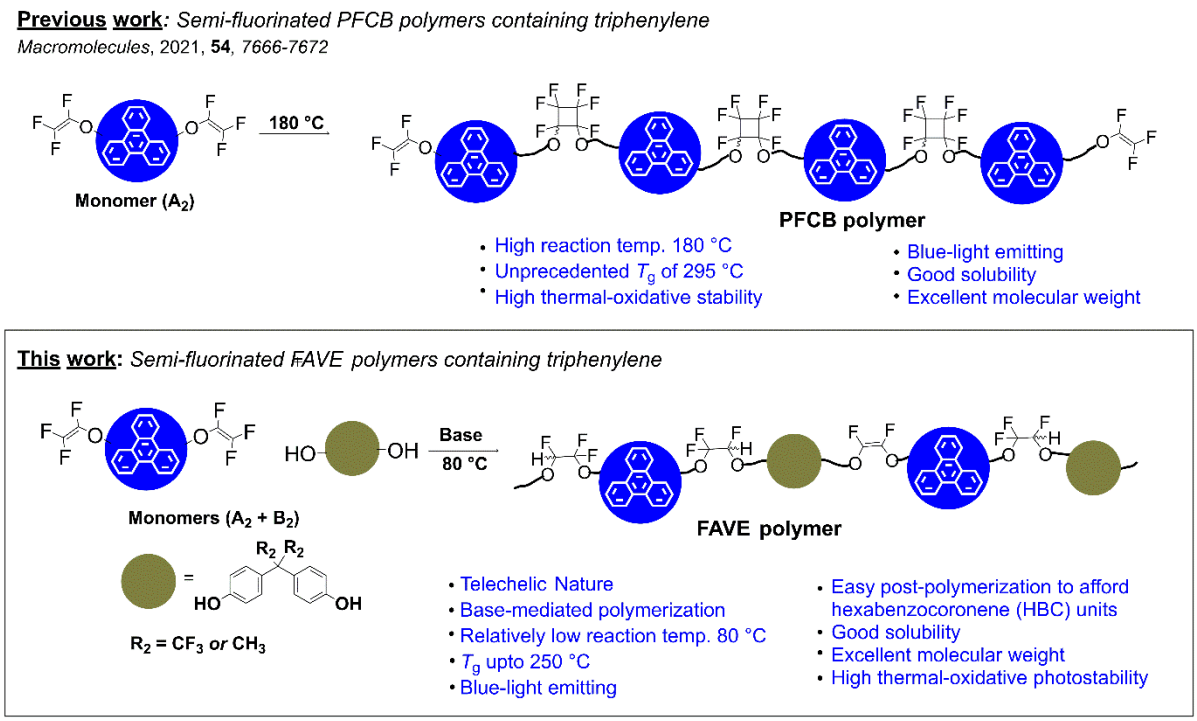

Figure 1. Semi-fluorinated polymers containing polycyclic aromatic hydrocarbon (PAH) core, triphenylene.

Readily available phenanthrenequinone was used to synthesize *bis*-TFVE variably substituted triphenylene monomers. The relative ease of preparing the polymers from *bis*-TFVE and bisphenol monomers,[56] the ability to tailor the polymer properties by varying spacer groups[57] and changing substitution on the triphenylene core offer the potential for structure/property control in monomers make this chemistry versatile. Finally, these polymers can be post-polymerized by chain extension and crosslinking of terminal phenol or TFVE end groups or crosslinking via the internal fluoroalkenes functions.[52,58] Additionally, we also report post-polymerization emission tunability of polymer **P3'** via Scholl coupling[59,60] that resulted in graphene-like planar hexabenzocoronene (HBC) core segments.

Results and discussion

Monomers **M1-M2** (as shown in Scheme 1) were synthesized using a literature procedure reported by our group.[54] Scheme S1 in the supplementary information (SI) illustrates the reaction sequence employed to afford monomers **M1** and **M2**, including the intermediate compounds **1**-**8**. Briefly, self-Claisen condensation of ethyl 4-bromophenylacetate **1** was performed to afford ethyl 2,4-*bis*(4-bromophenyl)-3-oxobutanoate **2**, followed by hydrolysis and decarboxylation which generated 1,3-*bis*(4-bromophenyl) acetone **3**. Subsequent double Knoevenagel condensation of **3** with available phenanthrenequinone **4** produced ketone **5**. Cyclopentadienone **5** was reacted with phenyl and diphenyl substituted alkynes via Diels-Alder addition/decarbonylation reactions to afford 1,4-*bis*(4-bromophenyl)triphenylene derivatives **6-7**. Suzuki-Miyaura coupling with *para*-boronic ester **8**, obtained from corresponding commercially available 4-bromotrifluorovinyloxybenzene **9** (Scheme S2), gave monomers **M1-M2** in good yields (73-79%). Detailed procedures and characterization including ^{1}H-, ^{19}F-, and ^{13}C-NMR analyses for **M1**, **M2** and their novel polymers **P1-P4** and **P1' -P4'** are described in the supplementary information. The

HR-MS and ATR-FTIR values of intermediates **1**-**8** and monomers **M1** and **M2** were previously presented.[54]

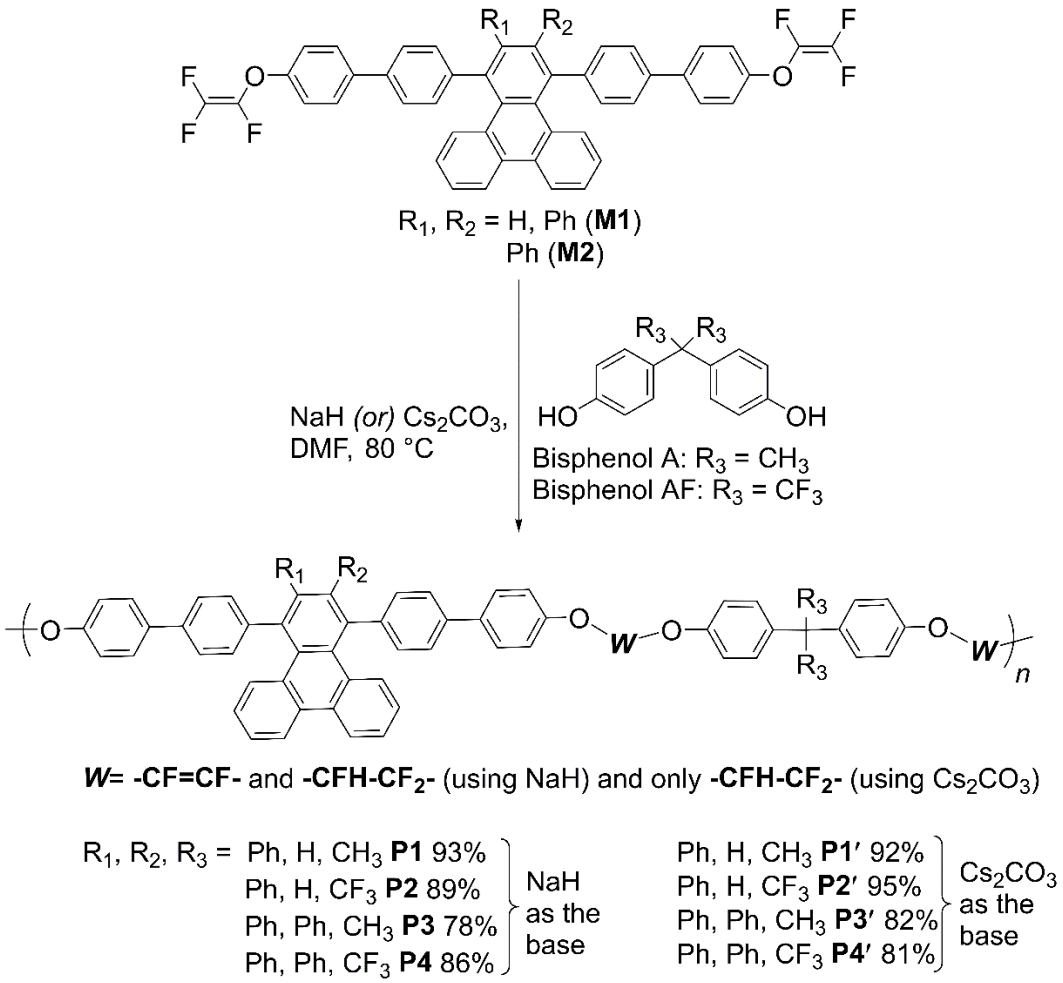

Scheme 1. Step-growth polymerization of *bis*(trifluorovinyloxy) triphenylene core derivatives (**M1**-**M2**) with bisphenols A and AF leading to polymers **P1**-**P4 (**using NaH) and **P1' -P4'** (using Cs_2CO_3).

Base-mediated step-growth polymerization of **M1** and **M2** (Scheme 1) with commercially available bisphenol A or bisphenol AF produced triphenylene-enchained semi-fluorinated thermoplastic FAVE polymers **P1**-**P4 (**using NaH) and **P1'**-**P4'** (using Cs_2CO_3) in 78-95% isolated yields after precipitation into CH_3OH/H_2O (50:50). The FAVE polymers each contain an all *para*-substituted pentaphenylene chain structure rarely reported within a soluble polymer. Nucleophilic

addition of phenoxide across TFVE functional groups gives the anionic intermediate -CF_2-:CF-, which can be protonated to give the –CF_2-CFH- linker. When anhydrous NaH is the base, some HF is eliminated to form the -CF=CF- alkene linker group (***W)*** in **P1**-**P4**. However, only -CF_2-CFH- linkages (***W***) are formed in **P1'-P4'** when the base is Cs_2CO_3.[61] Initial polymerization conditions were chosen based on previous studies of base and solvents for polymerization of TFVE-containing monomers with bisphenols.[55,61–64] While forming the fluorinated arylene vinylene ether (FAVE) polymers, Cs_2CO_3 provides saturated semi-fluorinated polymers with only –O-CFH-CF_2-O- linkages and NaH generates -O-CF=CFO- links with both the *E*- and *Z*-configurations by partial HF elimination.[65]

Gel permeation chromatography (GPC) was used for molecular weight analysis in THF versus polystyrene standards for each of the eight polymers (Table 1). The choice of the base played a key role in the polymerization mechanism and the resulting molecular weight distributions. All precipitated polymers exhibited PDI values from 1.2 to 1.8 with molecular weights from 38 to 57 kDa. Higher molecular weights were generally observed for polymers obtained when NaH was used as a base (42-57 kDa) compared with using Cs_2CO_3 (38-46 kDa). Overall, the number average molecular weight (M_n) values using either base ranged from 35 to 60 kDa. For example, **P1**, obtained from polycondensation of **M1** with bisphenol-A (BPA) and NaH, gave M_n of ~57 kDa with a PDI value of 1.6 after precipitation.

The solid-state ATR-FTIR spectra of monomers **M1** and **M2** exhibited a small characteristic stretching band for the ArO-CF=CF_2 double bond at 1832 cm^{-1}.[51,54] The polymers **P1**-**P4** and **P1'-P4'** were also characterized by ATR-FTIR experiments (Figures S1 and S2) which showed vibrations resembling: Ar/C=C stretching (1650-1500 cm^{-1}), C-F stretching (1100-1000 cm^{-1}), sp^2 C-O stretching (1350-1200 cm^{-1}), and sp^3 C-O stretching (~1000-850 cm^{-1}) bands. The

sharp peak observed at around 1000 cm^{-1} could also belong to 1,2-disubstituted aromatic ring C-H out-of-plane bending. Multiple strong signals from 900-700 cm^{-1} are consistent aromatic ring out-of-plane bending vibrations. The above assigned ATR-FTIR absorbances were further confirmed by the DFT Hessian computations. For example, the computationally predicted sp^3 C-O stretch of polymer **P1'** is at 1177 cm^{-1}. Additionally, in polymer **P1**, the computed sp^2 C-O stretch of *Z*-isomer of FAVE is at 1315 cm^{-1}, whereas the *E*-isomer peak appears at 1334 cm^{-1}.

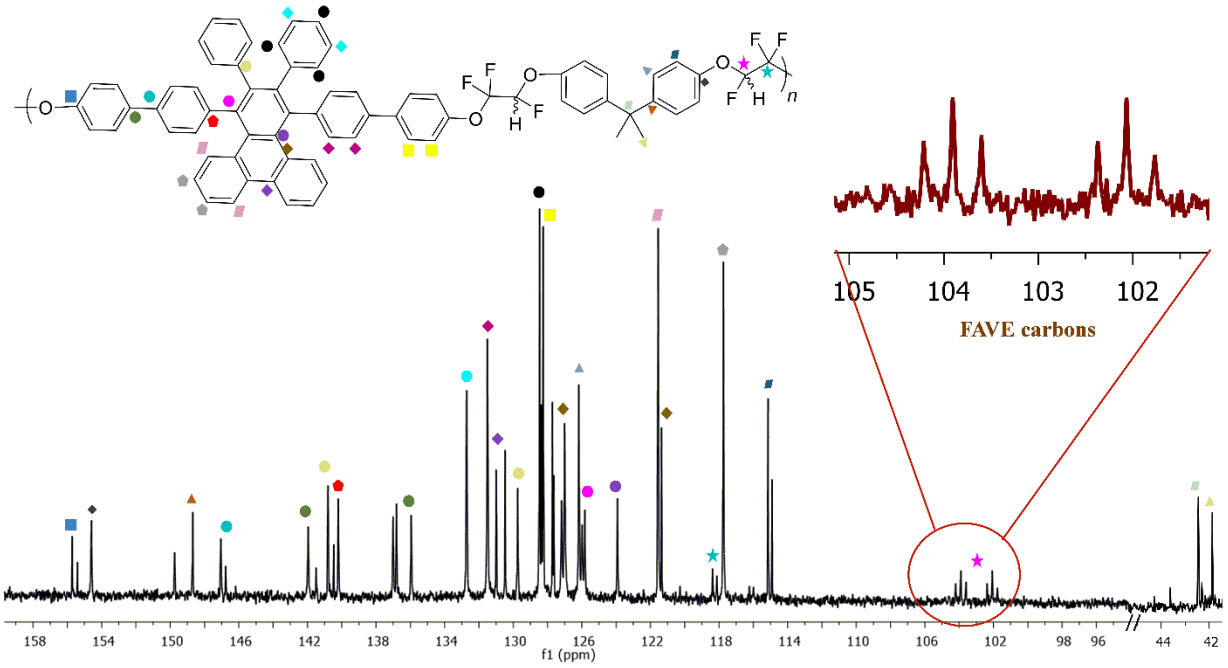

Figure 2. ^{13}C-NMR (in $CDCl_3$) spectra of polymer **P3'**.

Figure 2 displays the ^{13}C-NMR spectrum with individual peak assignments for polymer **P3'**. The presence of fluorocarbon FAVE linkages in **P3'** was evident by the C-F geminal and vicinal coupling from 105 to 101 ppm as a doublet of triplets (dt) with coupling constants (*J*) of 231.84 and 37.80 Hz as shown in Figure 1 (inset).

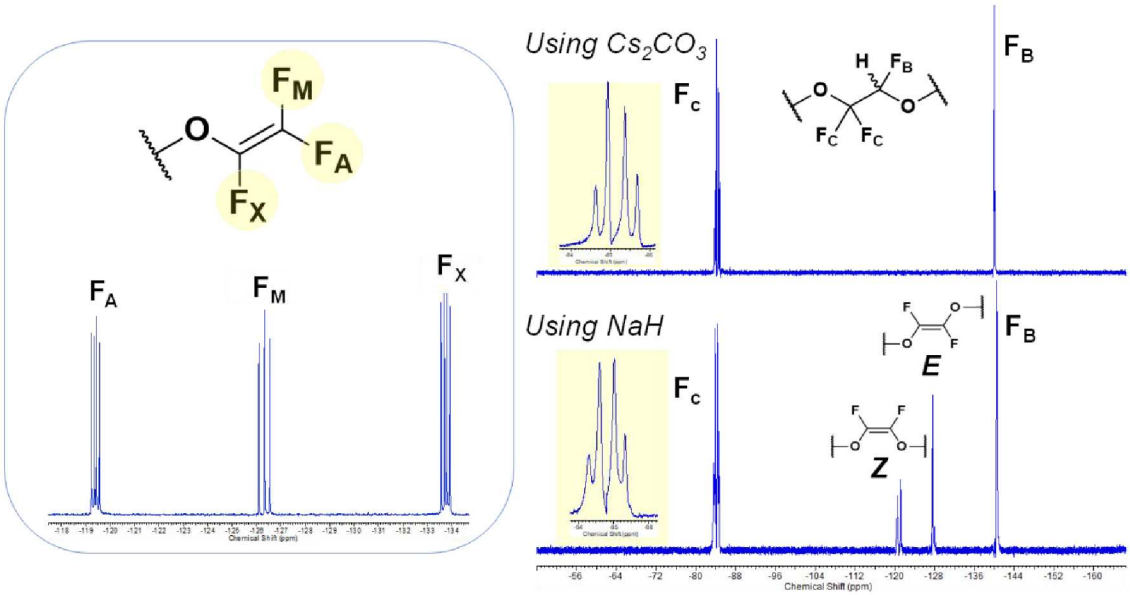

Figure 3. ^{19}F-NMR (in DMSO-d_6) spectra: monomer **M2** (left box), polymer **P3'** (top, using Cs_2CO_3) and polymer **P3** (bottom, using NaH) with ^{19}F-NMR peak integration of 1.05:1 ratio of (*Z*)/(*E*) isomers.

As step-growth polymerization of **M2** proceeds, the conversion of the trifluorovinyl ether (TFVE) and phenolic functional groups were followed by the disappearance of the well-known ^{19}F-NMR AMX pattern[66] (Figure 3 left box) of the -OCF=CF_2 group at -120.9 ppm (F_A), -128.2 ppm (F_M), and -135.5 ppm (F_X). As polymer **P3'** formed (using Cs_2CO_3), a well-defined doublet-of-doublets (dd) for geminal fluorine's (-O-C(F_C)$_2$-) appears at -85 ppm, and the lone fluorine (-CF_BH-O-) gives a broad splitting pattern near -141 ppm (Figure 3 top and bottom). Polymerization using the Cs_2CO_3 base gives exclusively polymers **P1'-P4'** bearing hydro-1,2,2-trifluoroethyl (***W*** = -CHF-CF_2-) bridges. Polymers **P1-P4** containing 1,2-difluorovinylene (both *Z/E* configuration for –CF=CF-) enchainment were prepared using sodium hydride with the %***W*** ranging from 12-21% (see Table 1). Attempts to increase the unsaturation using potassium *t*-butoxide or LDA, surprisingly, did not perform better than NaH for these polymers. ^{19}F-NMR spectrum (Figure 3 bottom) illustrates the *Z*-isomer (around -121 ppm) and *E*-isomer (around -128 ppm). In addition to the unsaturated fluorinated arylene vinylene ether (FAVE) peaks in the ^{19}F-NMR spectra of **P3**,

hydro-1,2,2-trifluoroethyl bridges (***W*** = -CHF-CF_2-) were also observed and are difficult to avoid completely (Figure 3 bottom).

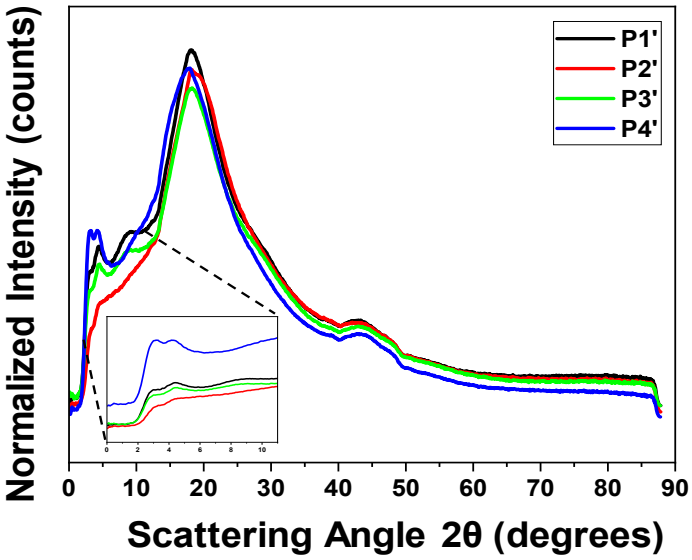

Figure 4. Powder XRD for polymers **P1'-P4'**.

Powder X-ray diffraction (XRD) studies (Figure 4) were performed on representative polymers **P1'-P4'**. The first peak at 2θ ~4° (20-28 Å) is attributed to the molecular diameter of the substituted PAH triphenylene core. Many other reported triphenylene-containing molecules show a similar diffraction peak around 5°.[67–69] Figure 4 (inset) illustrates slight differences in the ordering pattern of each polymer with varying core substitution. The intense, broad peak at 2θ ~18° (d-spacing = ~4.8 Å) is attributed to π-π stacking as expected. The d-spacing for ~18° peak resembles a vertical interlayer distance between the stacked cores of different or the same polymer chains. Thus, the appearance of several pairs of sharp arcs in the low-angle region indicate the existence of structures ordered on the nanometer scale. In the low-angle region, two peaks emerge for polymers **P1'-P3'** with d-spacings around 28.5 and 20 Å, however, those peaks are sharp in polymer **P4'**. In the wide-angle region, polymer **P2'** exhibits two diffused reflections centered at 4.6-4.8 Å (Figure S6-S13, Table S1-S4).

Thermal properties

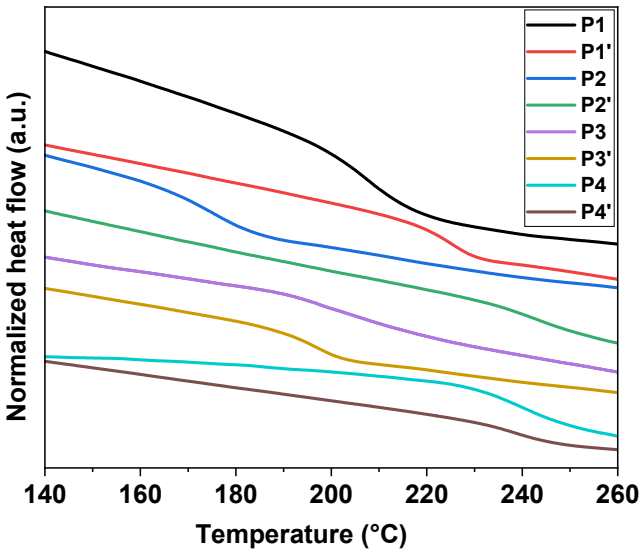

Figure 5. Fourth DSC heating cycles performed at 10 °C/min under nitrogen for semi-fluorinated polymers **P1**-**P4** and **P1'**-**P4'**.

The thermal properties of **P1**-**P4** and **P1'**-**P4'** were examined by DSC (Figure 5) and TGA (Figure 6). A surprisingly wide-range of glass transition temperatures (T_g's) were reproducible over four DSC heating cycles with no other events observed. The T_g values for polymers **P1**-**P4** and **P1'**-**P4'** were observed from 176 to 243 °C (Table 1). **P1**-**P4** and **P1'**-**P4'** have T_g values of about 100-200 °C greater than those with only bisphenols A or bisphenols AF (which range from 34 to 122 °C[56]). This demonstrates the ability of the large PAH core to anchor segmental motion, perhaps partially by the stacking interactions. Diphenyl substituted polymers **P3**, **P4**, **P3'**, and **P4'** do not show significant difference in T_g with change in bisphenol structure and degree of unsaturation. However, monophenyl substituted polymers **P1**, **P2**, **P1'**, and **P2'** are affected greatly by unsaturation, bisphenol and triphenylene substitutions. The presence of saturated fluorinated linkages in polymers **P1'** and **P2'** greatly increases the T_g when compared with its unsaturated polymer analog **P1** and **P2**, such as 208 vs. 224 and 176 vs. 243 °C.

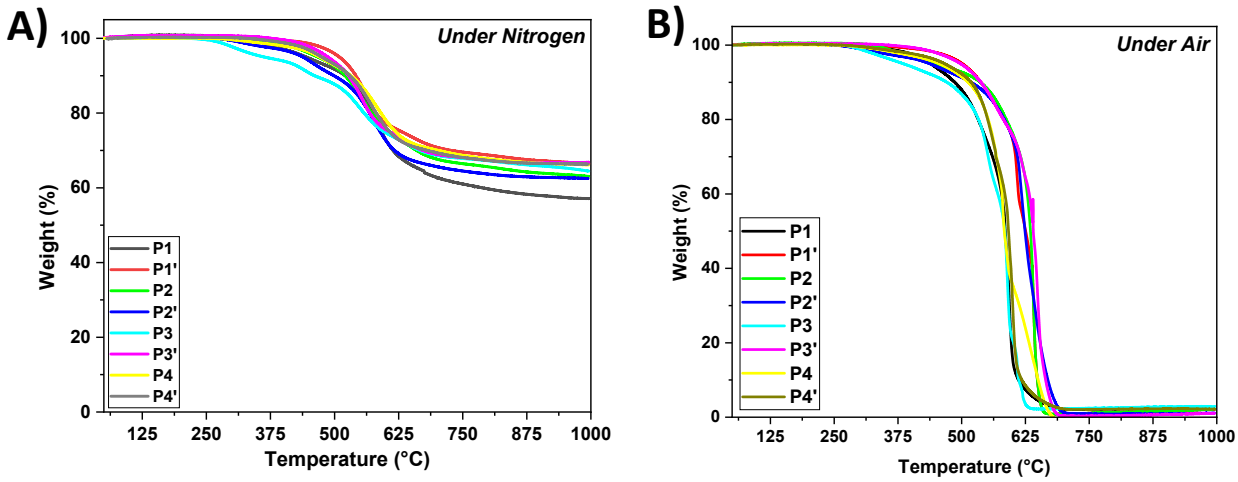

Figure 6. TGA thermal decompositions of FAVE polymers under nitrogen (left) and air (right).

TGA analyses of **P1**-**P4** and **P1'**-**P4'** gave high thermal stabilities in nitrogen and air (Figure 6). These semi-fluorinated polymers, each containing PAH cores, have higher thermal stabilities (T_g and T_d) than those FAVE polymer analogs obtained only using bisphenol A or bisphenol AF.[56] In addition to high temperature requirements during fabrication, thermally labile organic compounds can degrade during use in optoelectronic devices, such as OLEDs, due to Joule heating. This heating drives both thermal decomposition and oxidation in the organic layers, leading to defects, morphological changes, and mobile impurities.[70] Therefore, the established high thermal stabilities for these triphenylene FAVE polymers promote their eligibility as candidates for potential applications requiring optoelectronic device processing temperatures.

Table 1. Selected properties of the PNA-core containing **M1** and **M2** semi-fluorinated polymers versus those with only bisphenols monomers.

Entry[a]	Molecular weight[b]		%*W* = CF=CF[c]	T_g (°C)[d]	Temp. at 5% wt. loss (°C)[e]		Yield at 800 °C (%)[f]		T_d (°C)[g]	
	M_n x10^{-3}	M_w/M_n			N_2	Air	N_2	Air	N_2	Air
P1	57	1.6	17	208	468	440	66	2	638	603
P1'	46	1.2	-	224	510	502	69	0	617	646
P2	42	1.7	12	176	444	445	60	1	643	648
P2'	38	1.4	-	243	438	436	64	0	636	658
P3	54	1.8	21	208	376	375	67	3	619	601
P3'	41	1.3	-	197	490	496	67	1	623	662
P4	48	1.5	20	241	470	456	68	0	651	615
P4'	44	1.6	-	238	477	465	67	2	639	626

[a]**P1-P4** and **P1'-P4'** polymer structures containing **M1** or **M2** are shown in Scheme 1. [b]GPC in THF relative to polystyrene standards. [c]determined by ^{19}F-NMR peak integration; about 1.05:1 ratio of (*Z*)/(*E*) isomers. [d]DSC (10 °C/min) in nitrogen, third heating cycle. [e]5% weight losses were obtained by TGA under N_2 or air. [f]The char yield (at 800 °C) were obtained from the TA TGA instrument under N_2 or air for **P1-P4** (NaH, base) and **P1'-P4'** (Cs_2CO_3, base). [g]TGA onset at 10 °C/min.

Optical properties

The UV-vis absorption and fluorescence spectra of polymers **P1-P4** (solid lines) and **P1'-P4'** (dotted lines) are presented in Figure 7 and the data are summarized in Table 2. In the UV-vis absorption, all eight polymers exhibited three significant absorption bands in dichloromethane (DCM) between 200-300nm at 230, 260, and 298 nm (Figure 7A), indicating the different core substitutions did not significantly alter the excitation. It should be noted that the absorption maxima peak values obtained via experiment were compared with the computational results where the TD-DFT computations were performed for all polymers with one and two repeating units. These DFT computations further revealed the location of π-π* transitions in the polymer backbone (see section simulated spectra in supplementary information). The simulated spectra obtained from TD-DFT computations for polymers **P1-P4** and **P1'-P4'**also gave the same features with two peaks around 185 and 267 nm.

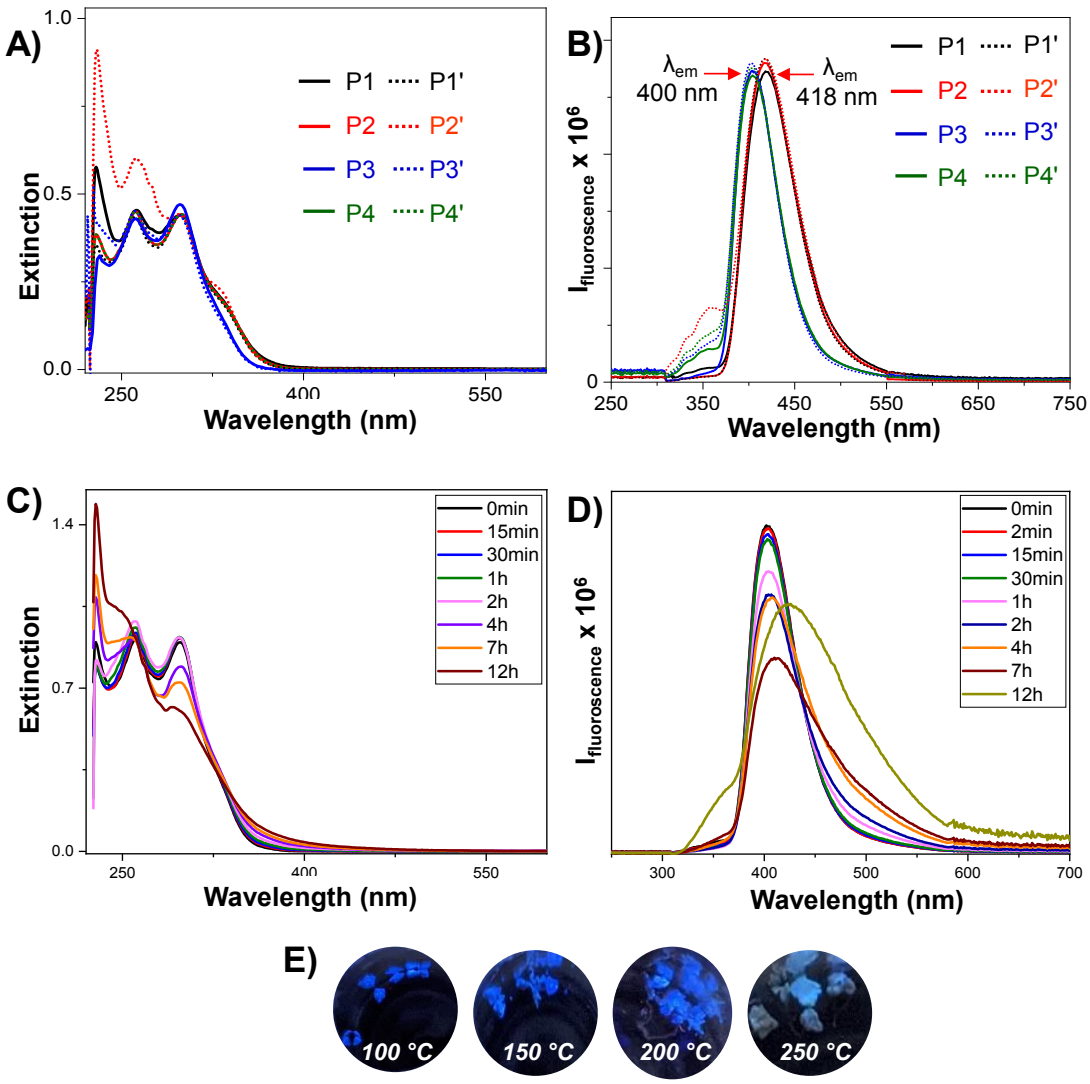

Figure 7. Overlay of the normalized spectra of **P1-P4** (solid lines) and **P1'-P4'** (dotted lines) at equal concentrations (4.5×10^{-5}M) in dichloromethane at temperature 25 °C: UV-vis extinction (A) and emission (B). Time-dependent study of polymer **P3'** when exposed to 254 nm UV-light: UV-vis extinction (C) and emission (D). Photographs of **P2'** powder irradiated (λ_{ex} = 365 nm) and heated to 100, 150, 200, and 250 °C in air for 1-5 h (E).

When exposed with a handheld UV lamp, each of the eight polymers generated intense blue photoluminescence in both solution and solid states. All fluorescence spectra (Figure 7B) were obtained by irradiating each polymer dissolved in DCM with a 298 nm excitation wavelength. The obtained emission maxima (λ_{em}) for **P1-P4** and **P1'-P4'** occurs from 400 to 420 nm. Polymers **P1**, **P1'**, **P2**, and **P2'** (R_1 = Ph, R_2 = H) exhibited peak emission maxima at 417-418 nm, while the

emission maxima for **P3**, **P3'**, **P4**, and **P4'** (R_1, R_2 = Ph) polymers were found at 403-404 nm (Table 2). The shape of each fluorescence emission spectrum for all eight semi-fluorinated polymers indicates that the emission peaks originated from the same excited state, despite the different R_1 and R_2 substitution and difference in λ_{em}. Polymers **P1**, **P1'**, **P2**, and **P2'** demonstrated bathochromic tailing in their UV-vis absorption spectra and ~14-15 nm red-shifts in fluorescence emission maxima indicating increased conjugation lengths when compared to **P3**, **P3'**, **P4**, and **P4'**. When the triphenylene core substituent R_2 is 'H', the R_1 phenyl substituent can lie coplanar to the core. However, both R_1 and R_2 are phenyl substituents in polymers **P3**, **P3'**, **P4**, and **P4'**, which leads to steric hindrance turning both phenyls out of the aromatic core's plane thereby decreasing the π-π conjugation and either raises the excited state energy or lowers the ground state (or both) for the polymers. The out-of-plane phenyl substituents caused a small blue shift of the experimental emission spectra in **P3** (404 nm) and **P4** (405 nm) vs. **P1** (417 nm) and **P2** (417 nm) (Table 2). These emissions can be compared with the λ_{em}= ~415 nm of the widely used blue emitter, dialkylpolyfluorene.[71] The saturated linkage in **P1'-P4'** and corresponding unsaturated FAVE polymers (**P1**-**P4**) gave essentially identical simulated absorption and emission spectra (see computational studies in SI). Nearly identical absorption and emission spectra were computed for **P1** and **P1'** despite the linker's unsaturation in **P1** (Table 2). The same trend was followed for polymers **P2** vs. **P2'**, **P3** vs. **P3'**, and **P4** vs. **P4'**.

The emission quantum yields for **P1**-**P4** and **P1'-P4'** were determined according to a reported method[72,73] (using quinine sulfate as a reference). Briefly, known concentrations of each polymer were prepared in DCM. Quinine sulfate was prepared in 0.1 M H_2SO_4. To eliminate the inner filter effect, the extinction values for the polymers and quinine sulfate solutions were held below 0.1. The photoluminescence quantum yields (Φ_{PL}) for these eight polymers ranged from 7.2

to 12% (Table 2). These values are consistent with the earlier reported values for FAVE polymers,[57] as well as triphenylene enchained PFCB polymers.[41]

Table 2. Optical properties of polymers **P1**-**P4** and **P1'**-**P4'** obtained experimentally (in DCM solution) and computationally (via DFT).

Polymer	λ_{abs} (nm)[a]		λ_{em} (nm)[d]		Φ_{PL} (%)[g]
	Computation[b]	Experiment[c]	Computation[e]	Experiment[f]	
P1	186, 267	264, 298	441	417	9.6±1
P1'	185, 267	261, 299	441	417	12±2
P2	186, 268	262, 299	443	417	11±1
P2'	183, 267	262, 297	437	418	10.6±1
P3	187, 264	262, 298	419	404	8.9±3
P3'	184, 267	262, 298	420	403	8.9±2
P4	187, 266	261, 299	413	405	8.3±1
P4'	185, 267	262, 297	422	405	7.2±2
HBC-P3*	194, 309	256, 325	320, 374	360, 382, 402	NA
Plausible side pdt.*	194, 309	256, 325	320, 374	360, 382, 402	NA

[a]Absorption maxima (λ_{abs}). [b]Computed by density functional theory (DFT) computations for polymers using one repeating unit at SMD (dichloromethane)-ωB97XD/BS1 level of theory (BS1 = 6-31G(d') for C, H, O and F). [c]Maximum absorbance peak in dichloromethane solution. [d]Emission maximum (λ_{em}). [e]Obtained from the computational excited state optimization process. [f]Peak emission using an excitation wavelength, $\lambda_{excitation}$ = 298 nm. [g]Fluoroscence quantum yield using quinine sulfate as a reference in 0.1 M H_2SO_4. *post-polymerized Scholl coupling desired product and plausible side product. See Scheme S3.

A polymer **P3'** solution in dichloromethane was exposed to a handheld UV-light (short wavelength 254 nm) to check its time-dependent photo-stability (Figure 7C and 7D). The UV absorption peaks exhibited a significant time-dependent hypsochromic shift after 12 h of UV-light exposure from 228, 262, 298 nm towards lower wavelength 228, 250, 294 nm indicating a loss in effective conjugation (Figure 7C). In contrast, the emission wavelength maximum and intensity of **P3'** were stable for up to 2 h yet showed a significant broad bathochromic emission shift from 403 nm to 426 nm after 12 h of UV-light exposure (Figure 7D).

Upon further study, polymer powders continued to emit blue light after heating to temperatures up to 250 °C in air for 1-24 h (Figure 7E). Polymer **P2'** powder was heated in air at 100, 150, 200, and 250 °C. The blue solid-state emission was maintained at all temperatures throughout the heating cycle and upon cooling to room temperature. After heating at 250 °C (above its glass transition temperature of 243 °C, see Table 1), a slight decrease in blue emission intensity was observed for the now crosslinked network.

Scholl coupling

Post-polymerization Scholl coupling was performed on polymer **P3'** to produce polymer **HBC-P3** containing hexabenzocoronene (HBC) units (Scheme S3). Two well-established Scholl reaction conditions were used employing (1) iron (III) chloride ($FeCl_3$)[74] or (2) 2,3-dichloro-5,6-dicyano-1,4-benzoquinone (DDQ)[75] to achieve cyclodehydrogenation of **P3'**. Quantitative ring closure to HBC was observed using DDQ, $MeSO_3H$ at room temperature, 20 min in DCM, while $FeCl_3$ produced only partial transformation even after 72 h (Figure S3). Limited attempts to optimize the reaction conditions using DDQ to increase the **HBC-P3** yield achieved little change in the product mixture. All reported Scholl coupling reactions reported (SI) used DDQ as the oxidant.

The ATR-FTIR trace (Figure 8) confirmed the formation of **HBC-P3**. The disappearance of multiple strong out-of-plane C-H bending modes at 1005, 826, 759, 727 cm^{-1} found in the fingerprint region for 1,4-disubstituted aromatic rings (1000-700 cm^{-1}) and the appearance of a new strong out-of-plane C-H bending signal at 735 cm^{-1} for 1,2,3-trisubstituted aromatic rings confirmed the hexabenzocoronene (HBC) nucleus.[76,77] Additionally, weak overtone bands (benzene fingers) typically observed in PAH at 1718 and 1675 cm^{-1} were observed in **HBC-P3**.

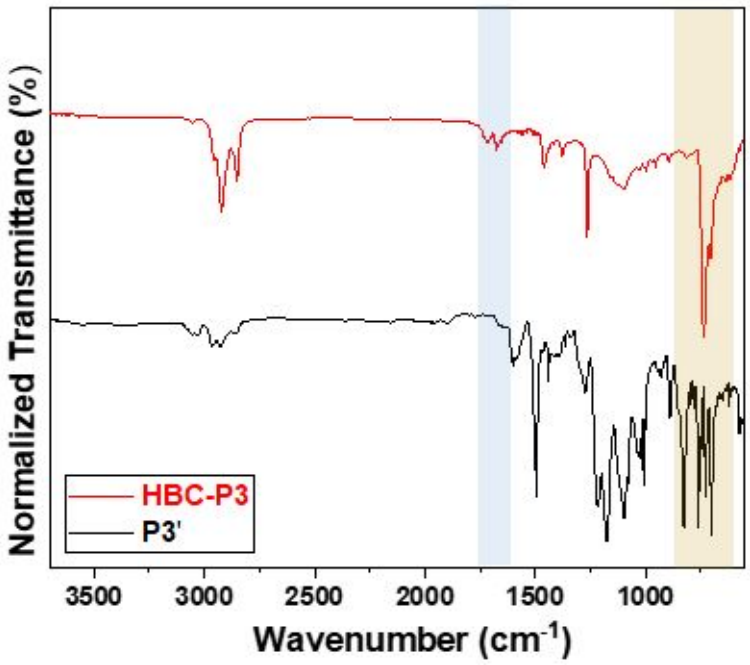

Figure 8. ATR-FTIR spectra: comparison of polymers **HBC-P3** (red) and **P3'** (black).

Figure S3 compares the ^{1}H-NMR spectrum of **P3'** and post-Scholl coupling product, **HBC-P3** (after workup). The ^{1}H-NMR spectrum of **HBC-P3** (Figure S3-top) no longer had proton peaks, due to the spin-spin coupling between adjacent protons, of **P3'**. These peaks disappeared upon the formation of **HBC-P3**. Importantly, the spectrum of **HBC-P3** featured a singlet at δ = 9.73 ppm which was previously reported to be a fingerprint signal for H_a in the expected graphene-like moiety of **HBC-P3**.[78,79] In addition, the aromatic region of the ^{1}H-NMR spectrum of **P3'** was shifted upfield in **HBC-P3** after the successful cyclodehydrogenation occurred. Due to an increased aromatic conjugation length, the protons H_b and H_c in **HBC-P3** (Figure S3 top) are more deshielded versus H_b' and H_c' in **P3'** (Figure S3 middle). Additionally, the ^{19}F-NMR spectra of **P3'** and **HBC-P3** (Figure S4) further confirmed the emergence of a new fluorine set within **HBC-P3** with an upfield shift of fluorine peaks represented as A' and B'. Along with our normal Scholl coupling polymer structure, another repeat unit structure was generated that shows a number of new ^{19}F-NMR fluorine signals in the hexabenzocoronene product mixture (Figure S4).

The Nucleus Independent Chemical Shift (NICS) computational method[80] was used to study the aromaticity of **HBC-P3** (Figure S14). This method calculates the chemical shift at specific locations in space around a molecule. The NICS value is an effective way to study the influences of induced ring currents of π electrons in an aromatic system. For polycyclic aromatic hydrocarbon (PAH) systems such as hexabenzocoronene (HBC), the NICS value can be obtained in analogous calculation of individual monocyclic rings present in the system in Figure S14A. All negative calculated chemical shifts from -19.6 to -33.8 ppm illustrate significant shielding effects around the HBC ring and support the description as an aromatic system. This data is consistent with prediction by Huckel's rule 4n+2 showing a 42 electron count. Figure S14A shows that the substituents in the left and right of the HBC imposes very small effect on the aromaticity, indicated by the identical NICS values in both rings (-24.0 ppm). The H_a protons of **HBC-P3** are the most deshielded protons with chemical shift value 9.73 ppm (Figure S3 top). The experimental results of **HBC-P3** are consistent with the values obtained via NICS computations revealing the H_a protons bearing phenyl rings shows the lowest NICS value -24 ppm (Figure S14A). However, NICS values in the polycyclic system should not be used alone to quantify the ring current between those individual rings because of the contribution of the neighboring ring.[81] For a more detailed study, NICS-XY-Scans (Figure S14B and S14C) were performed to calculate NICS values at various locations both above and in the plane of the ring. The vertical and horizontal scans gave three and five local minima (the most negative chemical shifts) respectively. The obtained local minima points were located in the center of the HBC ring. Thus, based on the shape of the scan HBC ring can be understood to have local aromaticity.[82]

Polarized optical microscopy (POM) of **HBC-P3** in dichloromethane (DCM) (4 mg/mL) was performed on a glass slide (Figure S5). The **HBC-P3**/DCM solution was sheared with a cover

glass and then heated at 50 °C for 15 min to remove the solvent. Further temperature was increased to 190 °C for 1 h, and POM at room temperature was performed. The hexabenzocoronene containing semi-fluorinated polymer, **HBC-P3**, reveals formation of definite textures exhibiting birefringence. A detailed POM study of triphenylene enchained polymers **P1-P4** and **P1'-P4'** is targeted for the future report.

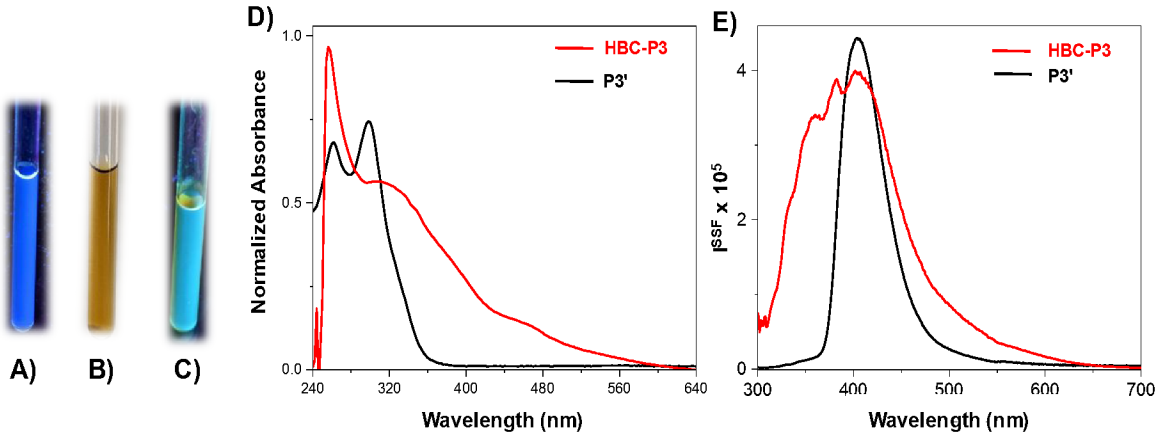

Figure 9. UV-light emission of polymer **P3'** (A), Scholl reaction product **HBC-P3** at visible light (B), UV-light emission of reaction mixture after Scholl coupling **HBC-P3** (C), UV-vis absorption of polymer **P3'** (black) and reaction mixture **HBC-P3** (red) (D), emission spectra of polymer **P3'** (black) and reaction mixture **HBC-P3** (red) (E).

Figure 9A and 9C reproduce the emission of polymers **P3'** and **HBC-P3** under UV light, while Figure 9B presents their emission under visible light. Figure 9D and 9E illustrate the UV-vis absorption and fluorescence spectra for polymers **P3'** and **HBC-P3**, respectively. A significant shift in absorption and emission wavelength (Figure 9D and 9E) is observed for Scholl product **HBC-P3** versus **P3'**. The 262 and 298 nm UV-absorption peaks of **P3'** changed to 256 (sharp) and 325 (broad) nm peaks in **HBC-P3**. Whereas 402 nm sharp emission maxima of **P3'** shifted to a broad emission peak (360, 382, and 402 nm) after Scholl coupling in **HBC-P3**. The core's conjugation in **P3'** increases after Scholl reaction afforded **HBC-P3**. Thus, a red emission shift was expected. Instead, a broad shift towards a lower wavelength was observed. To understand the

electronic structure differences, density functional theory (DFT) calculations were performed for **P3'** and **HBC-P3** (Table S6). The out-of-plane R_1 and R_2 phenyl substituents in **P3'** do not contribute to the excited transition due to their lack of conjugation to the planar core (see section simulated spectra in supplementary information). Figure S14 shows the comparison of computed energy diagram (eV) of frontier molecular orbitals of **P2'**, **P3'**, **HBC-P3**, and the plausible side product. However, after Scholl reaction, conjugation has been extended by the formation of the HBC core in **HBC-P3**. This new aromatic system creates significant change in the character of the UV-vis spectra. Figure S16 shows the computed energy diagram of before and after Scholl reaction. The Scholl coupling product generate higher excitation energy than **P3'** in both experimental and computational experiments (Table 2).

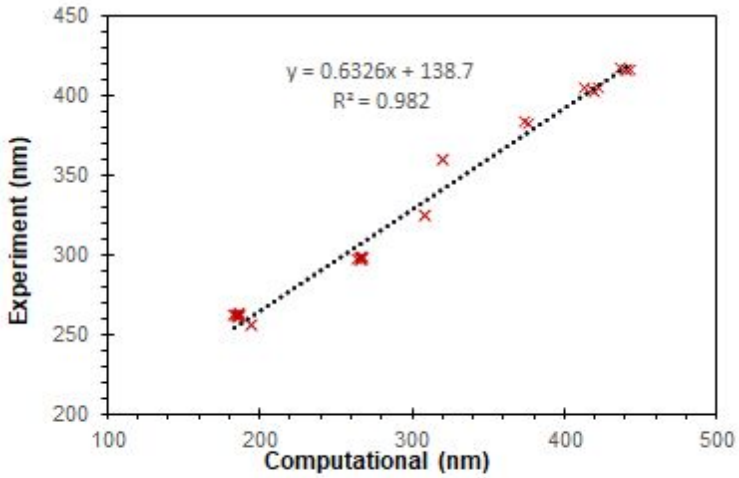

Figure 10. Correlation of absorption and emission peaks obtained via computational and experimental studies for polymers **P1**-**P4**, **P1'**-**P4'** and Scholl coupling product mixture.

The simulated absorption and emission spectra were created from computational results obtained from the DFT geometry optimized, singlet ground state structures and time-dependent density functional theory (TD-DFT) on the TD-DFT geometry optimized, first excited state singlet structures. For any particular structure, the computed transition energies are convoluted to produce a spectrum. Initially, the studies were performed on one model repeating polymer unit (made from

the condensation of two monomers, which corresponds to one repeating unit of the polymer). Subsequently, the polymer chain length was increased to two repeating units to examine the effect of polymer chain size on the accuracy of the computations. In DFT computations, increasing the number of repeating units in the polymer chain requires significantly more computation resources, especially the geometry optimization of the singlet excited state species. Increasing the polymer repeating units from one to two did give small differences in the simulated absorption and emission excitation spectra (Table S5). Increasing the polymer chain length with more than two repeating units leads to a set of intractable computations (semi-empirical geometry optimization computations may be performed, but semi-empirical methods provide much less reliable results). Interestingly, the differences in the computed transition energies for one or two repeating units are small. Therefore, because of the dramatically increased, impractical computational cost and the lack of an obvious advantage to the results with more repeating units, computations on larger oligomers were not performed (granted, the study is very limited on the number of repeating units that could be utilized). Aside from the polymer structure, the TD-DFT computational methodology may also lead to potential errors in the results, such as inaccurate geometries[83,84] and adiabatic approximation.[85] Thus, the values of the computed absolute excitation energies should not be compared directly to the experimental data; the trend in these results should be compared. As shown in Table 2, the computed UV-absorption λ_{abs} and emission λ_{em} values tend to be an underestimate when compared to those from the experiment. However, Figure 10 illustrates the excellent linear regression ($R^2 = 0.982$) between absorption and emission peaks when plotting the computational and experimental values of novel semi-fluorinated polymers **P1**-**P4**, **P1'**-**P4'** and Scholl coupling product mixture. This linear correlation demonstrates the systematic error that exists between the computed versus experimental results for this limited data set of semi-

fluorinated polymers. Based on these features, we conclude that the current level of theory carried out on one model repeating unit is adequate to represent the optical properties of the full polymers.

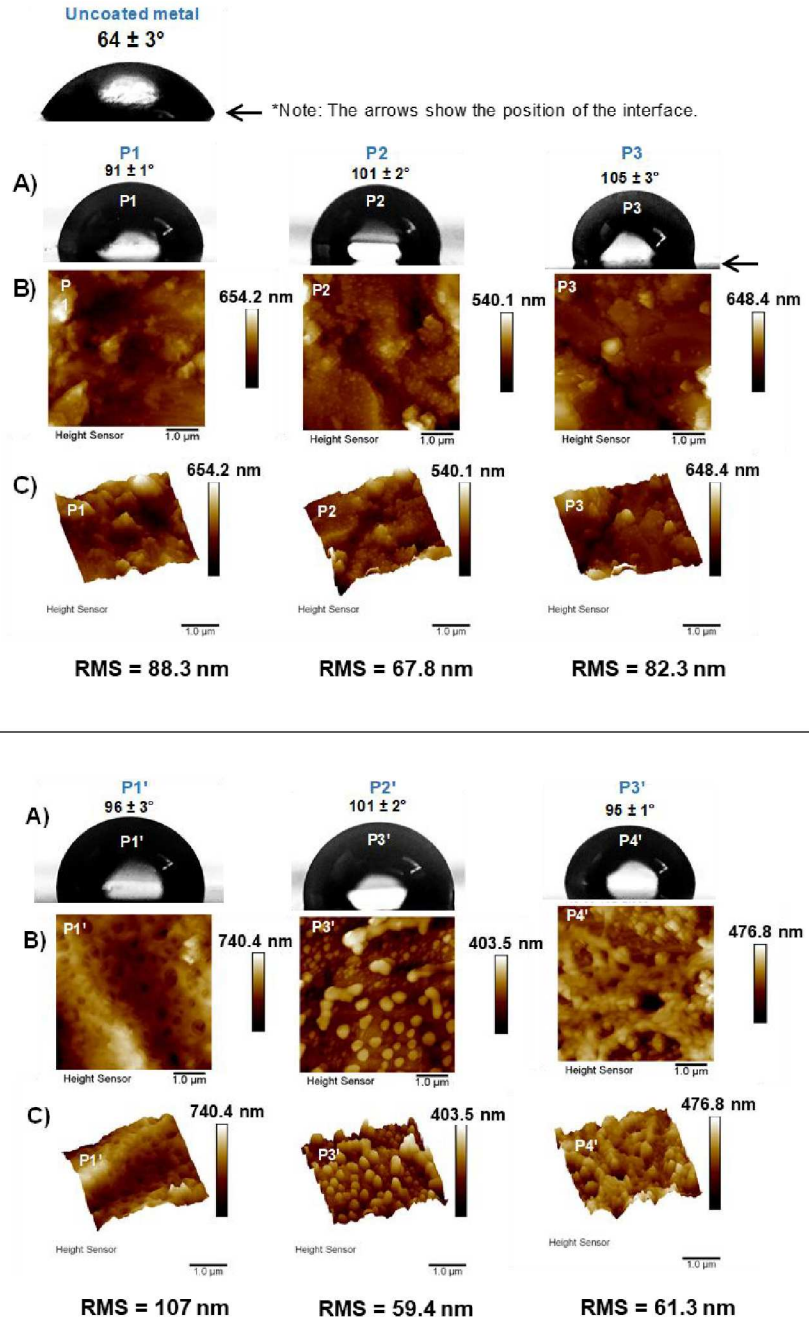

Figure 11. Water contact angles (CAs) (A), AFM 2D-images (5 × 5 µm) (B) and 3D-images (C) of **P1-P4** and **P1'-P4'** films on glass slides.

To assess the surface free energy and wettability, water contact angles (CA) were measured on the FAVE triphenylene polymer films prepared on stainless steel (SS) substrates. The water droplet images and the corresponding CA values are shown in Figure 11. In comparison to the bare metal substrate, the **P1-P4** and **P1'-P4'** triphenylene FAVE polymer-coated substrates displayed hydrophobicity with water CA values above 90°. Polymer **P3** exhibited the highest hydrophobicity with CA values of 105±3° for **P3** (Figure 11A). Such hydrophobic character indicates the fluoropolymers' potential protective property and inherently low surface free energy. The surface morphology was also studied for the same films on which the water CA's were measured. The root mean square (RMS) ranges from 59.4 to 107 nm. No correlation was observed between CA and RMS of triphenylene FAVE polymers. These polymers have a low surface roughness over an area of 5 μm^2 (Figure 11B and 11C).

Conclusion

Eight triphenylene-based semi-fluorinated FAVE polymers were synthesized via base mediated nucleophilic addition/elimination step-growth polymerization of commercial bisphenols with new triphenylene containing *bis*-trifluorovinyl ether (TFVE) monomers. The new high molecular weight FAVE materials were easily processed from solution and gave transparent free-standing films, exhibited excellent thermal stability (under both N_2 and air), and indicated high photo stability. The choice of base plays a crucial role in obtaining either a saturated (-CFH-CF_2-) or mixture of saturated (-CFH-CF_2-) and unsaturated (-CF=CF-, *E* and *Z*) fluorinated linkages. The polymers exhibited similar absorption ranges from 260 to 300 nm, with substitution dependent emission maxima at ~400 nm. These polymers are blue light emitters with DCM solution quantum yields from 7-12%. High T_g values up to 243 °C were measured by DSC, indicating that these materials may be promising candidates for optoelectronics and separation applications. Further

post-polymerization Scholl coupling (using DDQ as oxidant) generated the hexabenzocoronene (HBC) enchained FAVE polymer with new optical properties. Furthermore, the DFT computed and experimentally obtained absorption and emission values for all synthesized polymers showed excellent correlation with R^2= 0.982. Future study includes solid state photoluminescence quantum yields and establishing further structure/property relationships.

Author Contributions

Conceptualization, data curation, formal analysis, project administration, resources, writing-original draft, visualization, K.E.S.; formal analysis, software, N. L.; investigation, validation, K.E.S., N. L., K.M.M., S.D., S.A., B.D., E.C.; methodology, K.E.S., B.F.; writing-review & editing, K.E.S., C.U.P.J., C.E.D., D.W.S.J.; funding acquisition, C.E.D., D.W.S.J.; supervision, D.W.S.J.

Conflicts of interest

There are no conflicts to declare.

Acknowledgments

The authors would like to acknowledge the Department of Chemistry and The Advanced Composites Institute at Mississippi State University, Battelle Memorial Institute, and the NSF CHE 2102552 for supporting this project. Tetramer Technologies for the generous donation of TFVE starting materials. Additionally, we also thank Iwei Chu for her kind help in AFM experiments.

References

1 D. W. Smith, Jr., S. T. Iacono and S. S. Iyer, *Handbook of Fluoropolymer Science and Technology*, John Wiley & Sons, Inc., 2014.

2 S. Dolui, D. Kumar, S. Banerjee and B. Ameduri, Well-defined fluorinated copolymers:

current status and future perspectives, *Accounts Mater. Res.*, 2021, **2**, 242–251.

3 M. Guerre, G. Lopez, B. Améduri, M. Semsarilar and V. Ladmiral, Solution self-assembly of fluorinated polymers, an overview, *Polym. Chem.*, 2021, **12**, 3852–3877.

4 L. Xiao, Z. Chen, B. Qu, J. Luo, S. Kong, Q. Gong and J. Kido, Recent Progresses on Materials for Electrophosphorescent Organic Light-Emitting Devices, *Adv. Mater.*, 2011, **23**, 926–952.

5 Y. Jiang, Y. Y. Liu, X. Liu, H. Lin, K. Gao, W. Y. Lai and W. Huang, Organic solid-state lasers: a materials view and future development, *Chem. Soc. Rev.*, 2020, **49**, 5885–5944.

6 C. W. Tang and S. A. VanSlyke, Organic electroluminescent diodes, *Appl. Phys. Lett.*, 1987, **51**, 913–915.

7 M. H. Chua, Q. Zhu, K. W. Shah and J. Xu, Electroluminochromic Materials: From Molecules to Polymers, *Polymers*, 2019, **11**, 1–35.

8 J. H. Burroughes, D. D. C. Bradley, A. R. Brown, R. N. Marks, K. Mackay, R. H. Friend, P. L. Burns and A. B. Holmes, Light-emitting diodes based on conjugated polymers, *Nature*, 1990, **347**, 539–541.

9 A. M. Rice, E. A. Dolgopolova, B. J. Yarbrough, G. A. Leith, C. R. Martin, K. S. Stephenson, R. A. Heugh, A. J. Brandt, D. A. Chen, S. G. Karakalos, M. D. Smith, K. B. Hatzell, P. J. Pellechia, S. Garashchuk and N. B. Shustova, Stack the Bowls: Tailoring the Electronic Structure of Corannulene-Integrated Crystalline Materials, *Angew. Chem., Int. Ed.*, 2018, **57**, 11310–11315.

10 Y. Jiang, K. F. Li, K. Gao, H. Lin, H. L. Tam, Y.-Y. Liu, Y. Shu, K.-L. Wong, W.-Y. Lai, K. W. Cheah and W. Huang, Frequency-Upconverted Stimulated Emission by Up to Six-Photon Excitation from Highly Extended Spiro-Fused Ladder-Type Oligo(p-phenylene)s, *Angew. Chem., Int. Ed.*, 2021, **60**, 10007–10015.

11 Y.-M. Han, C. Sun, L.-B. Bai, J.-Y. Lin, M. Xu, Y.-Y. Liu, X.-H. Ding, L.-H. Xie, K. Shen, T.-S. Qin and W. Huang, Photoexcitation Dynamics of Thiophene–Fluorene Fluorophore in Matrix Encapsulation for Deep-Blue Amplified Spontaneous Emission, *ACS Appl. Polym. Mater.*, 2021, **3**, 1306–1313.

12 A. C. Grimsdale and K. Müllen, in *Emissive Materials Nanomaterials*, Springer, Berlin, Heidelberg, Berlin, Heidelberg, 2006, 1–82.

13 W. Zhao, M. Jiang, W. Wang, S. Liu, W. Huang and Q. Zhao, Flexible Transparent Supercapacitors: Materials and Devices, *Adv. Funct. Mater.*, 2021, **31**, 2009136.

14 L. Huang, Z. Wang, J. Chen, B. Wang, Y. Chen, W. Huang, L. Chi, T. J. Marks and A. Facchetti, Porous Semiconducting Polymers Enable High-Performance Electrochemical Transistors, *Adv. Mater.*, 2021, **33**, 2007041.

15 L. Xu, H. Wang, X. Feng, Y. Zhou, Y. Chen, R. Chen and W. Huang, Vanadium Oxide-Modified Triphenylamine-Based Hole-Transport Layer for Highly Reproducible and Efficient Inverted Perovskite Solar Cells, *Adv. Photonics Res.*, 2021, **2**, 2000132.

16 Q. Wei, Y. Li, J. Liu, Q. Fang, J. Li, X. Yan, L. Xie, Y. Qian, R. Xia and W. Huang, A High Performance Deep Blue Organic Laser Gain Material, *Adv. Opt. Mater.*, 2017, **5**, 1601003.

17 C. Li, M. Liu, N. G. Pschirer, M. Baumgarten and K. Müllen, Polyphenylene-Based Materials for Organic Photovoltaics, *Chem. Rev.*, 2010, **110**, 6817–6855.

18 J.-X. Chen, W.-W. Tao, W.-C. Chen, Y.-F. Xiao, K. Wang, C. Cao, J. Yu, S. Li, F.-X. Geng, C. Adachi, C.-S. Lee and X.-H. Zhang, Red/Near-Infrared Thermally Activated Delayed Fluorescence OLEDs with Near 100 % Internal Quantum Efficiency, *Angew. Chem., Int. Ed.*, 2019, **58**, 14660–14665.

19 L. N. Quan, B. P. Rand, R. H. Friend, S. G. Mhaisalkar, T.-W. Lee and E. H. Sargent, Perovskites for Next-Generation Optical Sources, *Chem. Rev.*, 2019, **119**, 7444–7477.

20 M. Usman, M. Munsif and A. R. Anwar, Wedge-shaped electron blocking layer to improve hole transport and efficiency in green light-emitting diodes, *Opt. Commun.*, 2020, **464**, 125493.

21 M. Usman, M. Munsif, U. Mushtaq, A.-R. Anwar and N. Muhammad, Green gap in GaN-based light-emitting diodes: in perspective, *Crit. Rev. Solid State Mater. Sci.*, 2020, **46**, 450–467.

22 A. Abdurahman, T. J. H. Hele, Q. Gu, J. Zhang, Q. Peng, M. Zhang, R. H. Friend, F. Li and E. W. Evans, Understanding the luminescent nature of organic radicals for efficient doublet emitters and pure-red light-emitting diodes, *Nat. Mater.*, 2020, **19**, 1224–1229.

23 W. Li, Q. Liu, Y. Zhang, C. Li, Z. He, W. C. H. Choy, P. J. Low, P. Sonar and A. K. K. Kyaw, Biodegradable Materials and Green Processing for Green Electronics, *Adv. Mater.*, 2020, **32**, 2001591.

24 C.-H. A. Li, Z. Zhou, P. Vashishtha, J. E. Halpert and J. E. Halpert, The Future Is Blue (LEDs): Why Chemistry Is the Key to Perovskite Displays, *Chem. Mater.*, 2019, **31**, 6003–6032.

25 Y. Wu, X. Li and H. Zeng, Highly Luminescent and Stable Halide Perovskite Nanocrystals, *ACS Energy Lett.*, 2019, **4**, 673–681.

26 J.-H. Lee, C.-H. Chen, P.-H. Lee, H.-Y. Lin, M. Leung, T.-L. Chiu and C.-F. Lin, Blue organic light-emitting diodes: current status, challenges, and future outlook, *J. Mater. Chem. C*, 2019, **7**, 5874–5888.

27 G. Grem, G. Leditzky, B. Ullrich and G. Leising, Realization of a blue-light-emitting device using poly(p-phenylene), *Adv. Mater.*, 1992, **4**, 36–37.

28 M. Fukuda, K. Sawada, S. Morita and K. Yoshino, Novel characteristics of conducting poly(9-alkylfluorene), poly(9,9-dialkylfluorene) and poly(1,10-bis(9′-alkylfluorenyl) alkane), *Synth. Met.*, 1991, **41**, 855–858.

29 J. Jo, C. Chi, S. Höger, G. Wegner and D. Y. Yoon, Synthesis and Characterization of Monodisperse Oligofluorenes, *Chem. – A Eur. J.*, 2004, **10**, 2681–2688.

30 M. Saleh, Y.-S. Park, M. Baumgarten, J.-J. Kim and K. Müllen, Conjugated Triphenylene Polymers for Blue OLED Devices, *Macromol. Rapid Commun.*, 2009, **30**, 1279–1283.

31 E. J. W. List, R. Guentner, P. Scanducci de Freitas and U. Scherf, The Effect of Keto Defect Sites on the Emission Properties of Polyfluorene-Type Materials, *Adv. Mater.*, 2002, **14**, 374–378.

32 S. S. Swayamprabha, D. K. Dubey, Shahnawaz, R. A. K. Yadav, M. R. Nagar, A. Sharma, F.-C. Tung and J.-H. Jou, Approaches for Long Lifetime Organic Light Emitting Diodes, *Adv. Sci.*, 2021, **8**, 2002254.

33 J. Huber, K. Müllen, J. Salbeck, H. Schenk, U. Scherf, T. Stehlin and R. Stern, Blue light-emitting diodes based on ladder polymers of the PPP type, *Acta Polym.*, 1994, **45**, 244–247.

34 T. P. I. Saragi, T. Spehr, A. Siebert, T. Fuhrmann-Lieker and J. Salbeck, Spiro Compounds for Organic Optoelectronics, *Chem. Rev.*, 2007, **107**, 1011–1065.

35 S. Kawano, C. Yang, M. Ribas, S. Baluschev, M. Baumgarten and K. Müllen, Blue-Emitting Poly(2,7-pyrenylene)s: Synthesis and Optical Properties, *Macromolecules*, 2008, **41**, 7933–7937.

36 J. Billard, J. C. Dubois, N. Huutinh and A. Zann, Mesophase of disc-like molecules, *Nouv. J. Chemie-New J. Chem.*, 1978, **2**, 535–540.

37 A. Bayer, S. Zimmermann and J. H. Wendorff, Low Molar Mass and Polymer Discotics: Structure, Dynamics and Opto-Electronic Properties, *Mol. Cryst. Liq. Cryst.*, 2003, **396**, 1–22.

38 I. Seguy, P. Destruel and H. Bock, An all-columnar bilayer light-emitting diode, *Synth. Met.*, 2000, **111–112**, 15–18.

39 N. Terasawa and H. Monobe, Alignment behaviour of symmetrical and asymmetrical triphenylenes possessing fluoroalkylated side chains on modified substrates, *Liq. Cryst.*, 2007, **34**, 447–455.

40 G. Heppke, D. Krüerke, C. Löhning, D. Lötzsch, D. Moro, M. Müller and H. Sawade, New chiral discotic triphenylene derivatives exhibiting a cholesteric blue phase and a ferroelectrically switchable columnar mesophase, *J. Mater. Chem.*, 2000, **10**, 2657–2661.

41 J. W. Levell, A. Ruseckas, J. B. Henry, Y. Wang, A. D. Stretton, A. R. Mount, T. H. Galow and I. D. W. Samuel, Fluorescence Enhancement by Symmetry Breaking in a Twisted Triphenylene Derivative, *J. Phys. Chem. A*, 2010, **114**, 13291–13295.

42 M. Saleh, M. Baumgarten, A. Mavrinskiy, T. Schäfer and K. Müllen, Triphenylene-Based Polymers for Blue Polymeric Light Emitting Diodes, *Macromolecules*, 2010, **43**, 137–143.

43 A. Rose, C. G. Lugmair and T. M. Swager, Excited-State Lifetime Modulation in Triphenylene-Based Conjugated Polymers, *J. Am. Chem. Soc.*, 2001, **123**, 11298–11299.

44 A. Vitale, R. Bongiovanni and B. Ameduri, Fluorinated oligomers and polymers in

photopolymerization, *Chem. Rev.*, 2015, **115**, 8836–8866.

45 B. Ameduri and B. Boutevin, *Well-Architectured Fluoropolymers: Synthesis, Properties and Applications*, Elsevier, 2004.

46 B. Améduri, The Promising Future of Fluoropolymers, *Macromol. Chem. Phys.*, 2020, **221**, 1900573.

47 D. W. Smith, Jr., S. Chen, S. M. Kumar, J. Ballato, C. Topping, H. V Shah and S. H. Foulger, Perfluorocyclobutyl Copolymers for Microphotonics, *Adv. Mater.*, 2002, **14**, 1585–1589.

48 E. B. Caldona, E. I. Borrego, K. E. Shelar, K. M. Mukeba and D. W. Smith, Jr., Ring-Forming Polymerization toward Perfluorocyclobutyl and Ortho-Diynylarene-Derived Materials: From Synthesis to Practical Applications, *Materials*, 2021, **14**, 1486.

49 J. G. Drobny, *Technology of Fluoropolymers*, CRC Press LLC, Boca Raton, 2001.

50 B. K. Spraul, S. Suresh, S. Glaser, D. Perahia, J. Ballato and D. W. Smith, Jr., Perfluorocyclobutyl-Linked Hexa-peri-hexabenzocoronene Networks, *J. Am. Chem. Soc.*, 2004, **126**, 12772–12773.

51 B. Farajidizaji, K. E. Shelar, G. Narayanan, K. M. Mukeba, B. Donnadieu, C. U. Pittman, Jr., A. Sygula and D. W. Smith, Jr., Acenaphthylene-derived perfluorocyclobutyl aromatic ether polymers, *J. Polym. Sci., Part A: Polym. Chem.*, 2019, **57**, 1270–1274.

52 K. M. Mukeba, B. Faradizaji, K. E. Shelar, C. U. Pittman, Jr. and D. W. Smith, Jr., Semi–fluorinated arylene vinylene ether (FAVE) telechelic polymers from polycyclic aromatic hydrocarbon bisphenols and trifluorovinyl aryl ethers, *Polymer*, 2020, **209**, 122955.

53 G. Narayanan, B. Faradizaji, K. M. Mukeba, K. E. Shelar, M. De Silva, A. Patrick, B. Donnadieu and D. W. Smith, Jr., Perfluorocyclohexenyl (PFCH) aromatic ether polymers from perfluorocyclohexene and polycyclic aromatic bisphenols, *Polym. Chem.*, 2020, **11**, 5051–5056.

54 B. Farajidizaji, E. I. Borrego, S. Athukorale, M. Jazi, B. Donnadieu, C. U. Pittman, Jr. and D. W. Smith, Jr., Triphenylene-Enchained Perfluorocyclobutyl Aryl Ether Polymers: A Modular Synthetic Route to Processable Thermoplastics Approaching Upper Limit T_g and Photostability, *Macromolecules*, 2021, **54**, 7666–7672.

55 J. Wu, J.-H. Liou, C. Y. Shu, Y. Patel, R. Menon, C. Santucci, S. T. Iacono, D. W. Smith and B. M. Novak, Facile method towards functionalization of partially fluorinated polyarylethers via sequential post-polymerization modification, *React. Funct. Polym.*, 2015, **93**, 38–46.

56 S. T. Iacono, S. M. Budy, D. Ewald and D. W. Smith, Jr., Facile preparation of fluorovinylene aryl ether telechelic polymers with dual functionality for thermal chain extension and tandem crosslinking, *Chem. Commun.*, 2006, 4844–4846.

57 S. T. Iacono, S. M. Budy, J. D. Moody, R. C. Smith and D. W. Smith, Jr., Modular approach to chromophore encapsulation in fluorinated arylene vinylene ether polymers possessing tunable photoluminescence, *Macromolecules*, 2008, **41**, 7490–7496.

58 S. Keck, T. A. Knoerzer, D. W. Smith, Jr. and S. T. Iacono, Preparation of partially fluorinated aryl/alkyl vinylene ether polymers, *Polym. Int.*, 2013, **62**, 1485–1491.

59 H. Ito, Y. Segawa, K. Murakami and K. Itami, Polycyclic Arene Synthesis by Annulative π-Extension, *J. Am. Chem. Soc.*, 2019, **141**, 3–10.

60 M. Grzybowski, B. Sadowski, H. Butenschön and D. T. Gryko, Synthetic Applications of Oxidative Aromatic Coupling—From Biphenols to Nanographenes, *Angew. Chem., Int. Ed.*, 2020, **59**, 2998–3027.

61 J. Q. Buquoi, D. W. Smith, Jr. and S. T. Iacono, Kinetic study of semifluorinated arylene vinylene ether polymers, *J. Polym. Sci., Part A: Polym. Chem.*, 2011, **49**, 4441–4447.

62 J. Ding, X. Du, M. Day, J. Jiang, C. L. Callender and J. Stupak, Highly Fluorinated Poly(arylene alkylene ether sulfone)s: Synthesis and Thermal Properties, *Macromolecules*, 2007, **40**, 3145–3153.

63 S. C. Kettwich, B. R. Lund, D. W. Smith., Jr. and S. T. Iacono, Recent Advances in Partially Fluorinated Arylene Vinylene Ether (FAVE) Polymers, *ACS Symp. Ser.*, 2012, **1106**, 9–28.

64 D. K. Brown, J.-M. Cracowski, S. T. Iacono, K. Christensen and D. W. Smith, Jr., Preparation of biphenyl perfluorocyclobutyl (BP-PFCB) polyethylene glycol (PEG) copolymers by the formation of fluorinated arylene vinylene ether (FAVE), *Polym. Bull.*, 2015, **72**, 1393–1405.

65 D. K. Dei, B. R. Lund, J. Wu, D. Simon, T. Ware, W. E. Voit, D. MacFarlane, S. M. Liff and D. W. Smith, Jr., High Performance and Multipurpose Triarylamine-Enchained Semifluorinated Polymers, *ACS Macro Lett.*, 2013, **2**, 35–39.

66 D. A. Babb, B. R. Ezzell, K. S. Clement, W. F. Richey and A. P. Kennedy, Perfluorocyclobutane aromatic ether polymers, *J. Polym. Sci., Part A: Polym. Chem.*, 1993, **31**, 3465–3477.

67 M. Gupta and S. K. Pal, Triphenylene-Based Room-Temperature Discotic Liquid Crystals: A New Class of Blue-Light-Emitting Materials with Long-Range Columnar Self-Assembly, *Langmuir*, 2016, **32**, 1120–1126.

68 Y. Xiao, D. Zeng, L. M. Mazur, A. Castiglione, E. Lacaze, B. Heinrich, B. Donnio, D. Kreher, A. J. Attias, J. C. Ribierre and F. Mathevet, A new class of nanostructured supramolecular organic semiconductors based on intertwined multi-lamellar co-assemblies in π-conjugated liquid-crystalline side-chain polymers, *Polym. J.*, 2017, **49**, 31–39.

69 N. Terasawa, H. Monobe and K. Kiyohara, Mesomorphic phase transition behavior of novel triphenylene compounds possessing fluoroalkylated side chains, *J. Fluor. Chem.*, 2006, **127**, 954–961.

70 X. Li, F. Kang and M. Inagaki, Buckybowls: Corannulene and Its Derivatives, *Small*, 2016, **12**, 3206–3223.

71 C. D. Dimitrakopoulos and P. R. L. Malenfant, Organic Thin Film Transistors for Large

Area Electronics, *Adv. Mater.*, 2002, **14**, 99–117.

72 M. P. Sk and A. Chattopadhyay, Induction coil heater prepared highly fluorescent carbon dots as invisible ink and explosive sensor, *RSC Adv.*, 2014, **4**, 31994–31999.

73 J. R. Lakowicz, *Principles of Fluorescence Spectroscopy*, Springer US, 1999.

74 S. Kumar, D. C. Huang, S. Venkateswarlu and Y. T. Tao, Nonlinear Polyfused Aromatics with Extended -Conjugation from Phenanthrotriphenylene, Tetracene, and Pentacene: Syntheses, Crystal Packings, and Properties, *J. Org. Chem.*, 2018, **83**, 11614–11622.

75 D. Reinhard, F. Rominger and M. Mastalerz, Synthesis of Triphenylene-Based Triptycenes via Suzuki-Miyaura Cross-Coupling and Subsequent Scholl Reaction, *J. Org. Chem.*, 2015, **80**, 9342–9348.

76 IR Spectrum Table & Chart | Sigma-Aldrich, https://www.sigmaaldrich.com/technical-documents/articles/biology/ir-spectrum-table.html, (accessed 2 April 2021).

77 S. A. Sandford, M. P. Bernstein and C. K. Materese, The Infrared Spectra of Polycyclic Aromatic Hydrocarbons with Excess Peripheral H Atoms (Hn -PAHs) And Their Relation To The 3.4 And 6.9 μm PAH Emission Features, *Astrophys. J. Suppl. Ser.*, 2013, **205**, 8.

78 J. Wu, M. D. Watson and K. Müllen, The Versatile Synthesis and Self-Assembly of Star-Type Hexabenzocoronenes, *Angew. Chem., Int. Ed.*, 2003, **42**, 5329–5333.

79 R. Yamaguchi, S. Ito, B. S. Lee, S. Hiroto, D. Kim and H. Shinokubo, Functionalization of hexa-peri-hexabenzocoronenes: Investigation of the substituent effects on a superbenzene, *Chem. - An Asian J.*, 2013, **8**, 178–190.

80 P. V. R. Schleyer, C. Maerker, A. Dransfeld, H. Jiao and N. J. R. Van Eikema Hommes, Nucleus-Independent Chemical Shifts: A Simple and Efficient Aromaticity Probe, *J. Am. Chem. Soc.*, 1996, **118**, 6317–6318.

81 P. Bultinck, Critical analysis of the local aromaticity concept in polyaromatic hydrocarbons, *Faraday Discuss.*, 2006, **135**, 347–365.

82 A. Stanger, G. Monaco and R. Zanasi, NICS-XY-Scan Predictions of Local, Semi-Global, and Global Ring Currents in Annulated Pentalene and s-Indacene Cores Compared to First-Principles Current Density Maps, *ChemPhysChem*, 2020, **21**, 65–82.

83 J. Wang and B. Durbeej, How accurate are TD-DFT excited-state geometries compared to DFT ground-state geometries?, *J. Comput. Chem.*, 2020, **41**, 1718–1729.

84 J. Tao, S. Tretiak and J.-X. Zhu, Prediction of excitation energies for conjugated polymers using time-dependent density functional theory, *Phys. Rev. B*, 2009, **80**, 235110.

85 S. J. A. van Gisbergen, F. Kootstra, P. R. T. Schipper, O. V Gritsenko, J. G. Snijders and E. J. Baerends, Density-functional-theory response-property calculations with accurate exchange-correlation potentials, *Phys. Rev. A*, 1998, **57**, 2556–2571.